Journal of Sustainable Development of Energy, Water and Environment Systems

http://www.sdewes.org/jsdewes

Year 2026, Volume 14, Issue 3, 1140725

Original Research Article

Investigation of Process Feasibility and Mechanical Performance of Prosopis Juliflora Biobased Residue Materials for Additive Manufacturing

Mihreteab Kidanemariam Gebregewergs*[1,2] , James Wamai Mwangi[3], Kabini Karanja[3], Monnamme Tlotleng[4,5]

[1]Department of Mechanical Engineering, Pan African University Institute for Basic Sciences, Technology, and Innovation (PAUSTI), Nairobi, Kenya

[2]Raya University, Maichew, Ethiopia

[3]Department of Mechatronic Engineering, Jomo Kenyatta University of Agriculture and Technology (JKUAT), Nairobi, Kenya

[4]Instruments Research and Development Group, Measurement and Control Division, Council for Mineral Technology (MINTEK), Randburg, Johannesburg, 2194, South Africa

[5]Materials Science Innovation and Modelling Research Group, North-West University, Mahikeng, Mmabatho 2745, South Africa

e-mail: mihreteabkidanemariam@rayu.edu.et, jwamai@jkuat.ac.ke, kkabini@eng.jkuat.ac.ke, MonnammeT@mintek.co.za

Cite as: Gebregewergs, M. K., Mwangi, J. W., Karanja, K., Tlotleng, M., Investigation of Process Feasibility and Mechanical Performance of Prosopis Juliflora Biobased Residue Materials for Additive Manufacturing, J.sustain. dev. energy water environ. syst., 14(3), 1140725, 2026, DOI: https://doi.org/10.13044/j.sdewes.d14.0725

ABSTRACT

Biobased residues from agriculture and invasive plants can be used as cost-effective, sustainable alternative materials for additive manufacturing. This study investigates the feasibility of using Prosopis juliflora, an invasive and abundant species, as a feedstock for binder jetting and paste extrusion three-dimensional printing. Leaf, stem, and pod powders were characterized, and carboxymethyl cellulose was used as a binder in different formulations. Leaf and stem powders exhibited suitable powder properties, with stable powder-bed formation during binder jetting. In contrast, pods were sticky and tended to agglomerate, limiting their use in this process. Paste extrusion manufactured stable components for all fractions except at high binder ratios for pod-based materials. Mechanical testing showed maximum compressive strengths of 6.74 MPa, 10.17 MPa, and 4.64 MPa, and flexural strengths of 4.94 MPa, 13.45 MPa, and 9.44 MPa for leaf, stem, and pod samples, respectively. These findings demonstrate the potential of Prosopis juliflora residues as sustainable materials for additive manufacturing applications.

KEYWORDS

P. juliflora, Biobased material, Feasibility, Mechanical performance, Additive manufacturing.

INTRODUCTION

The development of new materials has been a focus of technological improvement and industrial advancement, serving as a source of innovation that contributes to manufacturing processes and product performance [1]. In recent decades, additive manufacturing (AM) or three-dimensional (3D) printing creates structures by adding material layer by layer from a Computer-Aided Design (CAD) model according to the desired design, and has grown to become a revolutionary fabrication technique [2]. AM is gradually recognized as a more

* Corresponding author

sustainable manufacturing method than conventional subtractive processes, enabling quicker design cycles and better material utilization [3,4]. The latest progress proves that the combination of computational optimization methods with AM techniques, such as hybrid AM systems driven by AI [5] and machine-learning-assisted parameter control [6], can help improve mechanical performance, minimize defects, and significantly enhance production efficiency. This kind of development signifies that AM has been moving towards highly intelligent and optimized manufacturing systems. Despite this technological advancement, most commercially available AM materials are petroleum-based polymers, energy-intensive metals, or synthetic composites associated with high energy demand, limited sustainability, and environmental burdens.

There has been a growing interest in recent studies to use biobased materials as AM feedstocks, driven by the necessity to decrease dependency on non-renewable and energy-intensive feed materials. Sekula *et al*. [7] using extrusion, High-Speed Sintering (HSS), and selective laser sintering (SLS), processed a biodegradable composite material consisting of a cellulose acetate propionate and microcrystalline cellulose for high-voltage electrical insulators and concluded that although the mechanical properties of the processed biopolymer were below industrial acceptance, the composite materials remain promising for sustainable manufacturing of high-voltage cellulose insulators. Complementary works further emphasize that developing low-cost waste-derived feedstocks can significantly improve material utilization rates and support circular economy principles in AM [8].

The application of biobased materials in AM is, however, difficult because of the irregular morphology of the particles, poor flowability, and sensitivity to moisture, especially in powder-based processes. Among the several AM techniques, binder jetting (BJT) and paste extrusion (MEX) are showing potential for the utilization of agricultural byproducts and invasive plant species as viable and low-cost alternative feed materials. BJT offers several advantages, including simple operation, high printing speed, good powder bed capacity, and the ability to tailor the microstructure and properties of the final part without requiring melting or extrusion [9,10]. In contrast, MEX requires careful control of binder content, paste viscosity, extrusion rate, and drying behavior, as these elements have a profound impact on the dimensional stability and mechanical performance of printed components [11].

Previous studies have investigated the use of biobased and waste-derived materials in both BJT and MEX processes. For instance, Micke *et al*. [12] investigated the use of water hyacinth, an invasive aquatic species in Kenya, as a feedstock in BJT and achieved parts with a compressive strength of 0.47 N/mm^2. Similarly, Khan *et al*. [13] examined waste algae powder in binder jetting, reporting a green density of 0.70 g/cm^3 and compressive strength of 1.3 N/mm^2. These findings support the feasibility of utilizing biobased residues in powder-based AM processes. In extrusion-based processes, Hussein *et al*. [14] explored the strength of printed parts composed of rice husk and an alginate binder through a modified MEX 3D printer. They pointed out that binder ratio and moisture content were significant parameters, which affect mechanical strength as well as dimensional accuracy. Andanje *et al*. [15] used recycled High-Density Polyethylene (rHDPE) with rice husks for composite filament development as feedstock for extrusion-based 3D printing technology. The research conducted by Bah *et al.* [16] produced sustainable composite filaments using rHDPE and cactus powder for Fused Filament Fabrication (FFF), demonstrating the applicability of agricultural residues in extrusion-based techniques.

In addition to the agricultural waste, utilizing invasive plant species in AM has gained attention. Prosopis juliflora (P. juliflora), being both abundant and invasive, shows great promise for transformation into valuable materials. This would not only facilitate an efficient means of controlling their spread but also yield economic and environmental benefits. Materialistically, P. juliflora is a fibrous material consisting mainly of cellulose (30-40%), hemicellulose (25-30%), and lignin (20-25%) along with other minor extractives and ash [17].

Recent studies have examined the utilization of P. juliflora using different methods. In the field of structural materials, Santhosh *et al*. [17] reported that adding rice husk to P. juliflora-epoxy composites improved the mechanical performance by approximately 45% relative to the unmodified composites. Subbiah *et al*. [18] synthesized the hybrid composite made up of P. juliflora and phoenix sylvestris fibers with the glass fiber and epoxy resin using the hand lay-up process, showing improved fiber-matrix bonding strength post alkali treatment. Apart from the structural purposes, Debella *et al*. [19] found that P. juliflora could be utilized as a promising material for biodiesel production, producing methyl esters which met the American Society for Testing and Materials (ASTM) biodiesel fuel standards. Furthermore, Rao *et al*. [20] produced a heterogeneous biochar-based catalyst using pyrolysis of P. juliflora biomass waste for biodiesel production. However, the previous studies focused on conventional processes such as composite fabrication and biodiesel production. To the authors' knowledge, no prior study has evaluated the printability of different P. juliflora plant fractions (leaves, stems, and pods) across different AM techniques.

The present study addresses this gap by evaluating the suitability of P. juliflora biobased residues as filler materials in BJT and MEX. The choice of leaf, stem, and pod fractions was motivated by the need to utilize the whole plant efficiently by processing each fraction separately, thereby enhancing material efficiency during biomass conversion. Each fraction exhibits unique morphological, flow and rheological properties, and binder interaction which greatly impact AM processability and final product performance [21].

The process of feasibility is assessed through indicators such as powder flowability, particle size distribution (PSD), morphology, powder-bed formation (for BJT), extrusion stability, and dimensional retention (for MEX). Since the present work focuses on preliminary powder characterization and powder-bed formation in BJT, detailed mechanical testing of binder-jetted parts is reserved for ongoing research involving experimental design and optimization. Mechanical evaluation in this study, therefore, focuses on paste-extruded components. The specific objectives of this study are to: (i) characterize the physical and flow properties of the P. juliflora powders for BJT, (ii) evaluate the printability of the residual materials under binder jetting conditions, (iii) develop and assess printable pastes to use in extrusion-based printing, and (iv) evaluate the mechanical properties of paste-extruded parts under varying volumetric flow rates and binder ratios.

MATERIALS AND METHODS

This section presents the materials used and experimental methods applied in the research work. It includes details on the collection and pre-processing of P. juliflora residues, powder preparation and characterization, process parameters selection, and mechanical testing of 3D printed components.

Material Description and Sample Collection

The P. juliflora species, originally from Central and South America, was intentionally brought to dry and semi-dry areas to help with land recovery and provide fuelwood [22,23]. It has since spread widely across Africa, Asia, the Middle East, and parts of Australia, where it's now often seen as an invasive species that brings about serious ecological and socio-economic issues [22]. For example, it forms dense thickets that reduce biodiversity, degrade grazing land, and lower water tables in affected regions [24]. However, despite these negative effects, its abundance offers a great chance for developing sustainable materials and utilizing them in new manufacturing technologies. Given its widespread presence, especially in arid and semi-arid regions, P. juliflora was chosen for this study as a source of biobased material. Figure 1, shows that the species has established dense stands in countries including Kenya, Ethiopia, Sudan, India, Pakistan, Australia, Brazil, Mexico, and the United Arab Emirates [25].

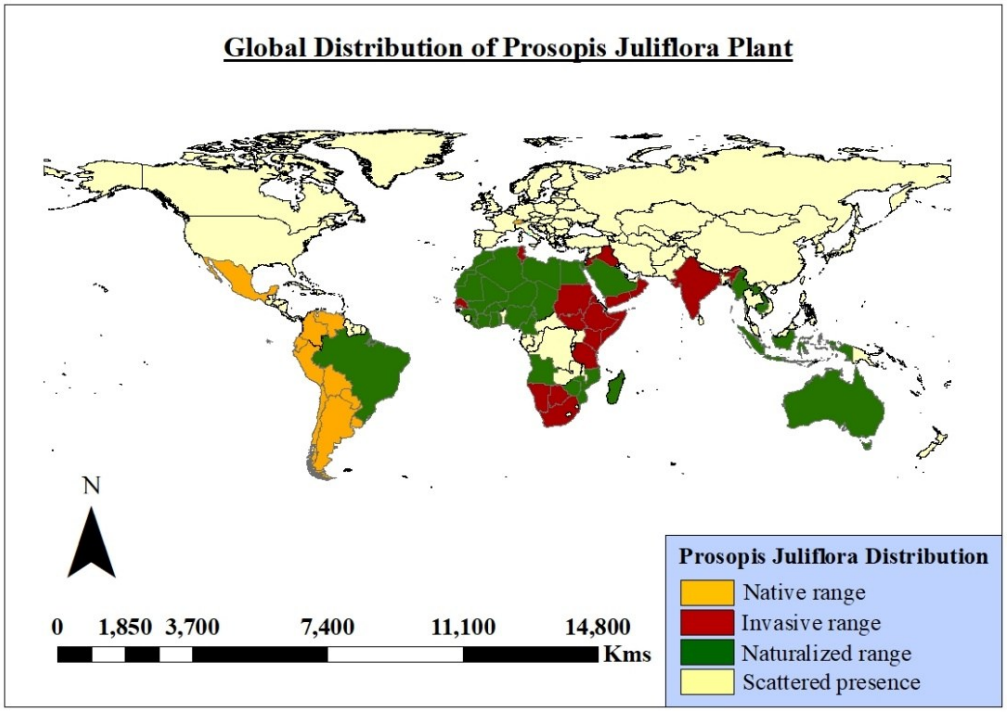

Figure 1. Global distribution areas of the Prosopis juliflora plant [25].

For experimental consistency, raw material was collected from Marigat in Baringo County, Kenya. Marigat is an area known for its high density of mature P. juliflora stands [26]. For clarity, the area-view of Marigat: the area from where the samples used in this study were collected, was self-reproduced and depicted in Figure 2. The biobased residues used for the AM processes were derived from the leaves, stems, and pods of the collected plants. Processing distinct parts helps to observe variations in powder properties that are crucial for effective powder spreading in BJT and paste behaviour in MEX processes.

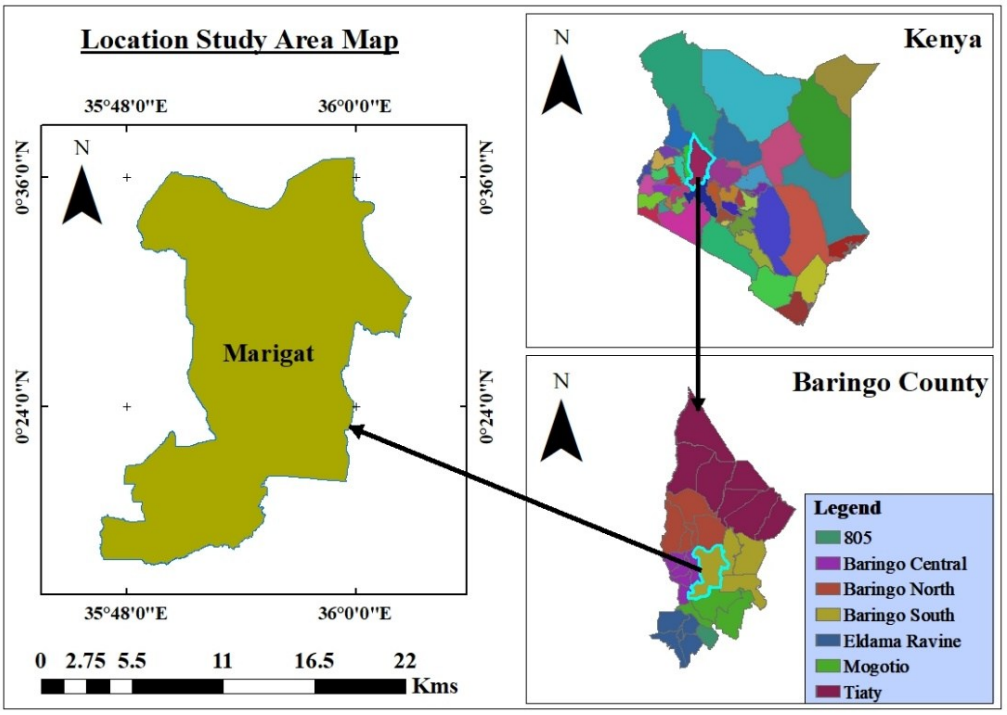

Figure 2. Location of the study area in Marigat, Baringo County, Kenya.

Material Pre-processing

The freshly obtained P. juliflora biobased residues were cleaned and washed to remove dust, dirt, and organic materials. All materials were dried in a closed solar dryer for seven days to mitigate environmental factors such as moisture. The daily average temperature and relative humidity inside the solar dryer were approximately 40 ± 5 ℃ and 50.7 ± 5%, respectively. Although the average temperature was moderate, peak mid-day temperatures of ~ 60 ℃ combined with low relative humidity (~22%), provided complete moisture removal without requiring external energy input. Pre-crushing of residues was performed using a hammer mill with a 1.5 kW power rating and an approximate throughput of 15 kg/h to reduce the materials into smaller particles for subsequent milling. Fine powders suitable for 3D printing were then produced by ball milling (4kW), obtaining approximately 6 kg of powder in 2 hours. Figure 3 illustrates the equipment used for drying and grinding in the study. These procedures resulted in a suitable fine powder for the BJT and MEX processes being achieved.

Figure 3. Equipment used for drying and grinding: (a) Solar dryer; (b) Hammer mill; and (c) Ball mill.

The overall pre-processing of P. juliflora residue materials into the range of printable powders were done at JKUAT, Kenya, as shown in Figure 4, with the corresponding flow diagram outlined in Figure 5.

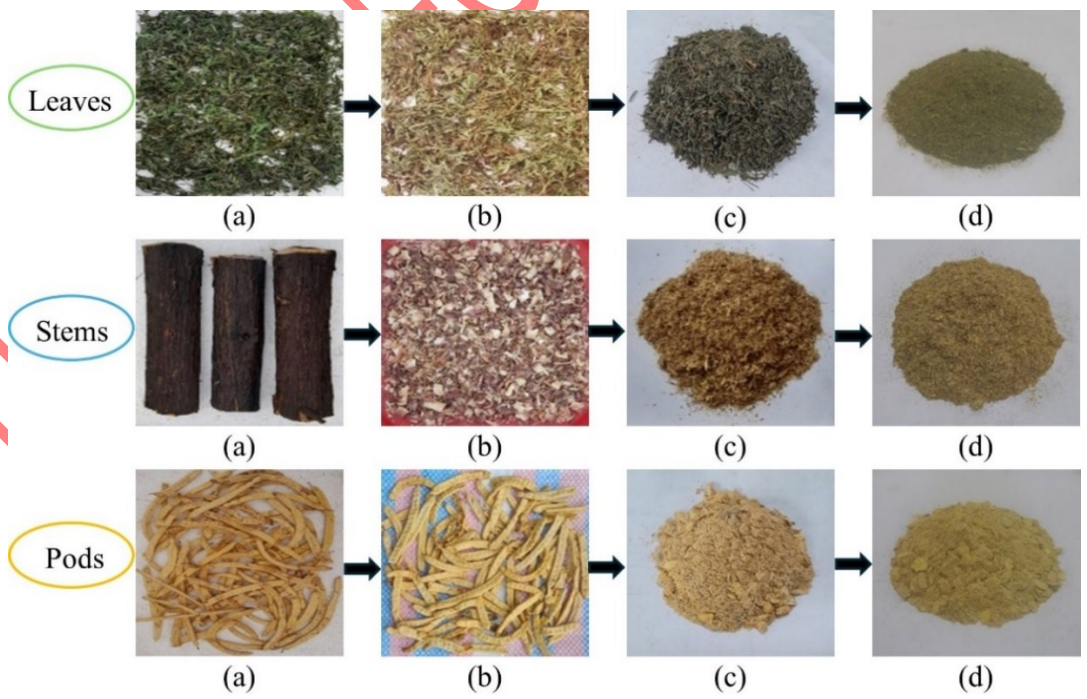

Figure 4. Pre-processing steps of residue materials: (a) Freshly harvested and cleaned; (b) After complete drying; (c) After crushing; and (d) After ball milling.

The energy required for the pre-processing operation was estimated based on the power rating of the machines used and the time taken for processing the materials and compared with literature values for conventional lignocellulosic biomass grinding. In this respect, the drying process was powered by solar energy, meaning that the external energy requirement for the drying process was insignificant. Energy requirements for mechanical grinding have been found to be between 0.1–0.5 kWh/kg and 0.5–2 kWh/kg for hammer milling and ball milling respectively. The reported values align with those in the literature [27], indicating lower energy demand than conventional thermal drying and high-energy milling processes.

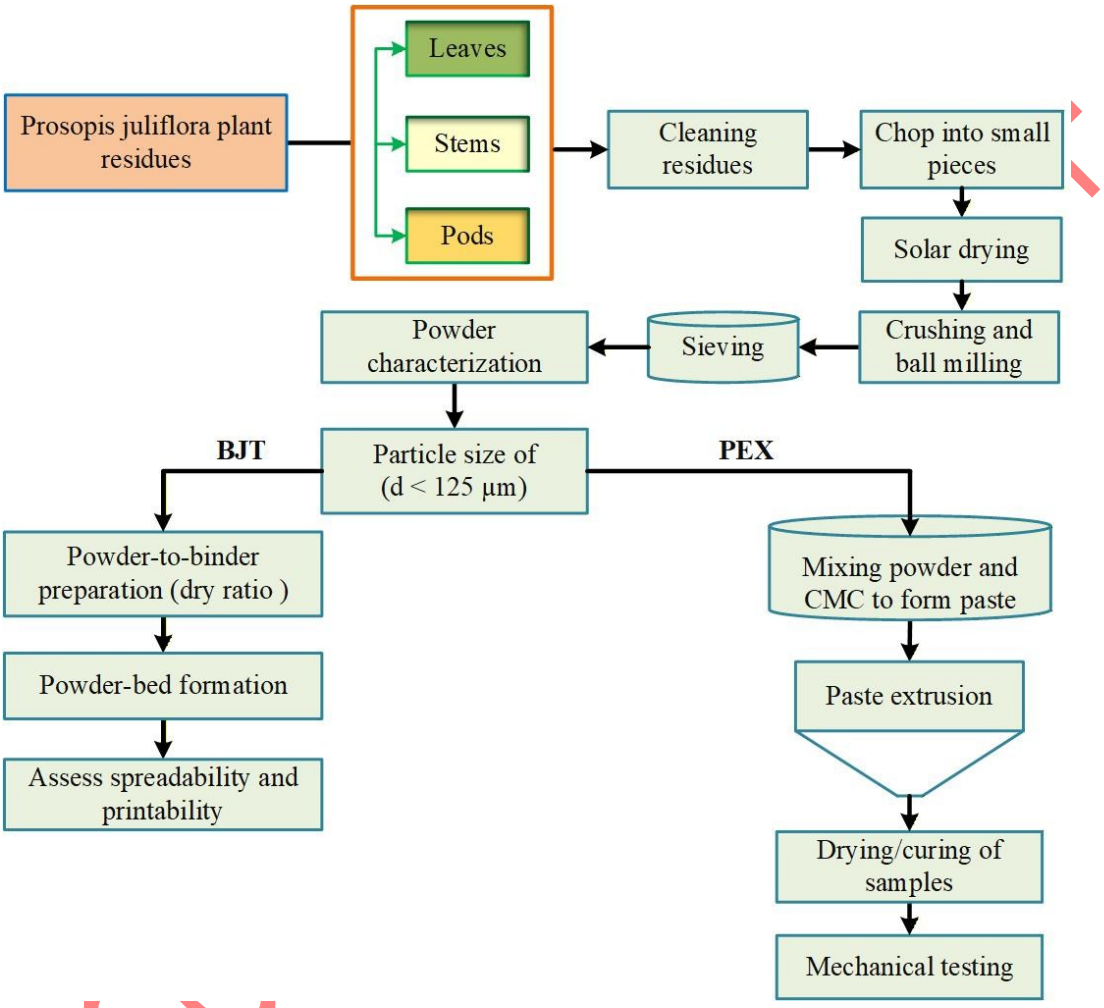

Figure 5. Flow diagram for the preparation, printing, and testing of residue powder materials.

Powder Characterization

The physical and morphological characteristics of P. juliflora powders were studied using a standard procedure at Jomo Kenyatta University of Agriculture and Technology (JKUAT) in Kenya. All measurements were carried out in triplicate, and average values are reported. Moisture content was determined using a KERN DAB moisture analyzer [28], as illustrated in Figure 6a. The bulk density of powders was measured according to (DIN ISO 60 "Art. No: 5346800") [29,30]. In every bulk density measurement, the mass of the empty density cup was first measured. Powder was then added to the funnel through the funnel opening, as in Figure 6b is narrower than the funnel. The powder is fed through gravity, filling the measuring cylinder under the funnel, forming a cone, and overflowing. The cone was carefully scraped off using a spatula, and the weighing cylinder holding the powder was weighed as shown in Figure 6c.

To determine the bulk density in each of the measurements, the net powder mass in the cylinder was divided by the volume of the cylinder (100 cm^3). Tapped density was measured using a JEL STAV II tapped density tester (J. ENGELSMANN AG) after a predefined number of taps until volume stabilization [31], as shown in Figure 6d.

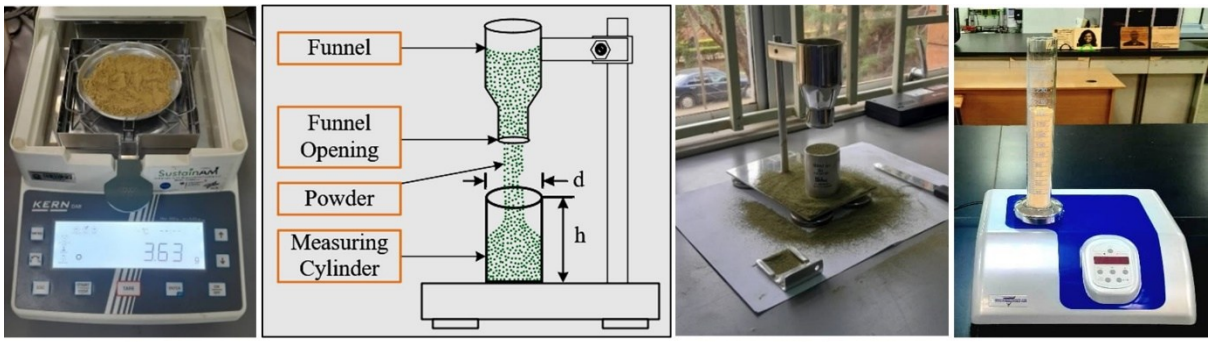

Figure 6. Measuring apparatus: (a) Measurement of moisture content; (b) Hall flowmeter setup; (c) Measurement of bulk density; and (d) Measurement of tapped density.

The flow properties and packing behaviour of the powder were evaluated using the Carr Index (CI) and Hausner Ratio (HR), calculated from bulk density (ρ_{bulk}) and tapped density (ρ_{tapped}) as per eq. (1) and eq. (2), respectively [32]:

$$CI = \left(\frac{\rho_{tapped} - \rho_{bulk}}{\rho_{tapped}}\right) x\ 100\ (\%) \quad (1)$$

$$HR = \frac{\rho_{tapped}}{\rho_{bulk}}\ (Unitless) \quad (2)$$

The flow behaviours of P. juliflora biobased powder fractions were classified based on the criteria proposed by powder-process.net and summarized in Table 1 [33].

Table 1. Classification of powder flowability based on CI and HR for BJT 3D printing.

Flow Character	Carr Index [%]	Hausner Ratio	Numerical rating [1-5]	Description of powder suitability
Extremely poor	> 38	> 1.60	1	Unsuitable for BJT
Very poor	32 – 37	1.46 – 1.59	2	Significant limitations
Poor	26 – 31	1.35 – 1.45	2-3	Marginally suitable
Passable	21 – 25	1.26 – 1.34	3	Acceptable for experimental use
Fair	16 – 20	1.19 – 1.25	3-4	Usable
Good	11 – 15	1.12 – 1.18	4	Suitable for printing
Excellent	< 10	1.00 – 1.11	5	Optimal flow for BJT

The powder fractions were morphologically characterized using a scanning electron microscope (SEM) [34] with a secondary electron detector (SED). All images were taken using high vacuum at an accelerating voltage of 15 kV, and a working distance of ~20 mm. Samples were mounted on conductive stubs and sputter-coated to avoid charging. SEM micrographs were obtained at different magnifications to have a clear observation of the shapes of the particles and surface textures. These observations provided essential insights into particle

morphology, which influences powder dispersion and spreading in the BJT process. The d < 125 µm particle size, common to all materials, was selected for PSD analysis and printing due to its balanced flow properties and preliminary trials of spreading and layer formation. PSD was conducted using a laser diffraction particle size analyzer (model: SALD-2300, No: I563258E0704).

Powder-Bed Formation in Binder Jetting

A preliminary evaluation of powder behaviour was done using printability trials with ZCorporation's "ZPrinter 310" 3D printer, as shown in Figure 7, at the Sustain AM laboratory in JKUAT. Small amounts of powder were loaded into the feed bed, and the spreading function was activated several times to spread a thin layer of powder from the feed bed onto the build bed. The resulting powder layers were then analyzed qualitatively for their uniformity, packing stability, and tendency to clump or segregate [35].

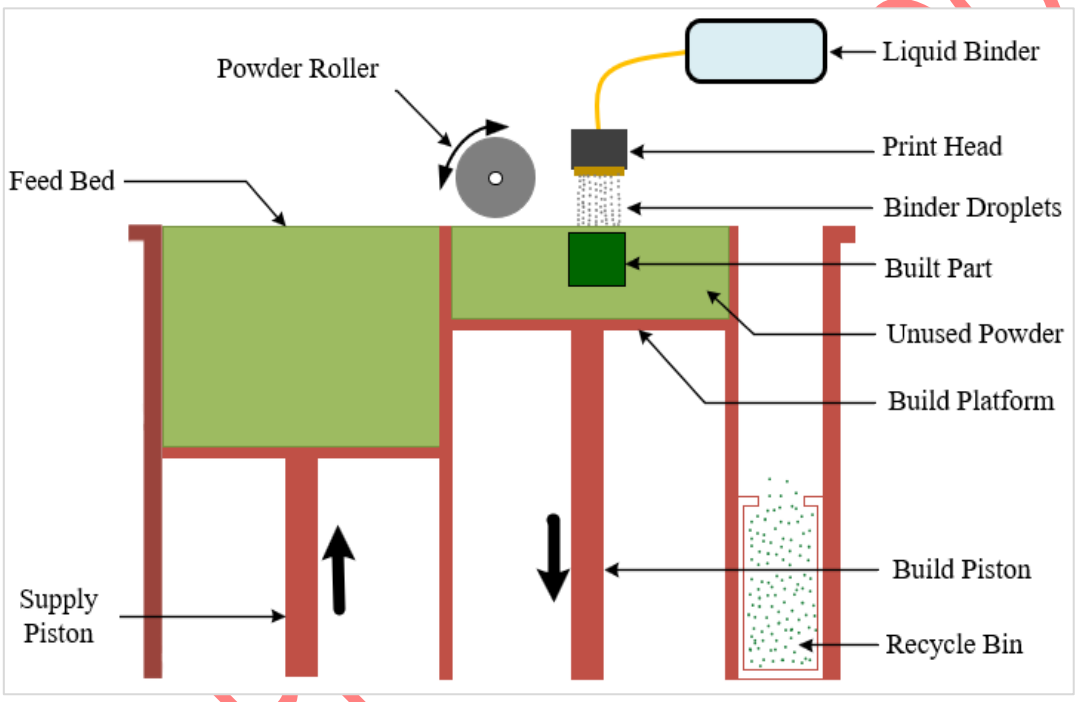

Figure 7. Schematic of the binder jetting using the "ZPrinter 310" 3D printer.

To further assess buildability, cubic specimens (20×20×20 mm^3) were designed in SolidWorks 2019 and printed with a layer thickness of 0.1 mm, approximately twice the mean particle size [13], a binder saturation of 120%, and a powder-to-binder (P/B) ratio of 85/15 (15 wt.% CMC) to balance particle adhesion and material efficiency [36]. Carboxymethyl cellulose (CMC) [37,38] were utilized as a solid binder. The liquid binder consisting of 100 mL of isopropanol, 50 mL of glycerin, 10 mL of liquid SDS, and distilled water (filled up to a total volume of 1 L) was also used for printing the parts. The printability of powders and the dimensional consistency of the green parts were visually analyzed.

Paste Printability and Sample Preparation Using Paste Extrusion

Paste formulation and preparation. As the P. juliflora powders are very absorbent and sticky, paste formulations were prepared by mixing the powder fractions with a water-soluble binder, CMC. Two P/B ratios, by weight percent, i.e., 85/15 (15 wt.% CMC) and 70/30 (30 wt.% CMC), were investigated for each material fraction. These ratios were selected to represent low and high binder contents within a practical processing range to assess the binder content effects on paste flowability, filament stability, and mechanical performance. Dry powders were first

homogenized to ensure uniform binder distribution. Water was then gradually added during manual mixing until a workable paste capable of continuous extrusion was obtained. Depending on the formulation and nature of the material, moisture content from 54% to 68% by total weight was used. The moisture content was not treated as an independent process parameter; rather, it was adjusted only to achieve extrudable consistency. Pre-tests of printability were conducted to assess if the paste could be easily extruded and form stable, continuous layers, and with reasonable dimensional accuracy. The printability evaluation focused on the influence of volumetric flow rate and P/B ratio on layer uniformity, dimensional stability, and mechanical performance rather than on the direct effect of moisture content.

3D printing. Test samples were manufactured using an in-house modified Creality Ender3 S1 printer adapted for paste extrusion, as shown in Figure 8. A nozzle with a diameter of 4 mm was used for printing, and the layer height was set to 2 mm using the Prusa Slicer software. For all test samples, the printing speed was fixed at 5 mm/sec to identify the effect of volumetric flow rate. Volumetric flow rate was selected as a key factor because it directly governs the amount of material deposited per unit time, influencing filament continuity, internal void formation, dimensional accuracy, and mechanical behavior [39]. Based on the results obtained from the preliminary testing for parameter screening, three different values of the volumetric flow rate were identified; these included: 40 mm^3/s, 52 mm^3/s, and 64 mm^3/s, which are equivalent to 100%, 130%, and 160% extrusion multipliers. Scenarios that resulted in nozzle clogging, discontinuous extrusion and excessive deformation were omitted.

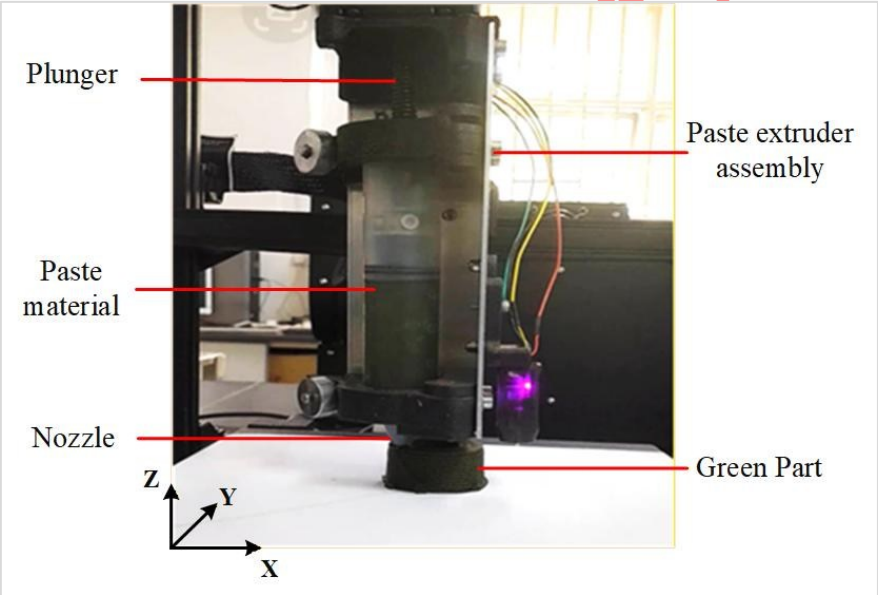

Figure 8. Paste extrusion 3D printing.

Two specimen geometries were designed for mechanical testing. For the compressive test, a hollow cylinder (outer diameter 40 mm, inner diameter 20 mm, and height 20 mm) was employed to improve dimensional stability during printing and drying, as solid cylinders have been reported to exhibit deformation and cracking due to moisture gradients and shrinkage in paste-extruded materials [14,40]. The hollow geometry enabled more uniform drying and reduced internal stresses, ensuring reliable and reproducible measurements. For flexural testing, rectangular bars (100 × 20 × 10 mm) were employed in a three-point bending test, consistent with ASTM D790 [41] which is commonly adopted in extrusion-based AM studies.

All printed test samples were dried under ambient laboratory conditions at room temperature (~25.6 °C). No additional curing or thermal post-processing was applied. Each combination of biobased fraction, binder ratio, and flow rate was printed in triplicate, and results were averaged. As summarized in Table 2, the printing parameters for manufacturing

samples were chosen per printer software and literature guidance to ensure reproducible mechanical performance [14].

Table 2. Printing parameters used for paste-extruding samples.

Printing parameter	Considered value
Extruder speed [mm/sec]	10
Printing speed [mm/s]	5
Nozzle diameter [mm]	4
Specimens layer height [mm]	2
Drying room temperature [°C]	~ 25.6

Mechanical Characterization of Paste-Extruded Parts

The printability and structural integrity of the paste-extruded samples were quantitatively evaluated through compressive and three-point bending flexural tests in JKUAT. For the compression test, the diameters and height of each hollow cylindrical specimen were measured prior to testing using a digital calliper. Compressive strength of specimens was analyzed according to ASTM D695 using a SHIMADZU universal testing machine (UTM). The specimen was placed on the testing platform. The crosshead speed was adjusted to 5 mm/min, and the loading anvil was then moved downwards until it contacted the upper surface of the specimen. Compressive load was subsequently applied until failure occurred. A force-displacement curve was recorded using TRAPESIUMX software. The compressive stress (σ_C) was calculated using eq. (3), where the load-bearing cross-sectional area was determined from the difference between the outer and inner circular areas of the hollow cylinder as:

$$\sigma_C = \frac{F_{max}}{\frac{\pi}{4}(D_0^2 - d_i^2)} (MPa) \quad (3)$$

where F_{max} is the maximum compressive load (N), D_0 is outer diameter (mm), and d_i is the inner diameter (mm) of the specimen.

In a similar way, flexural strength was conducted in a three-point bending system as per ASTM D790 of the same UTM. A digital calliper was used to measure all dimensions of the specimens before conducting the actual tests. Flexural loading was applied until failure, at which the loading nose was moved downwards at a constant crosshead speed of 5 mm/min to achieve contact of the nose with the specimen. The flexural strength (σ_f) was determined using eq. (4) of a rectangular bar cross-section:

$$\sigma_f = \frac{3F_{max}L}{2bh^2} (MPa) \quad (4)$$

where F_{max} is the maximum bending force (N), L is the span length (mm), h is the specimen thickness (mm), and b is the specimen width (mm).

RESULTS AND DISCUSSION

This section briefly discusses the results of the experiments conducted in the study. It analyzes the properties of the prepared powder materials, their effect on the printability in BJT and MEX techniques, and mechanical performance of the manufactured samples.

Powder Characterization

Biomass-based powder is highly susceptible to environmental conditions, which can influence moisture content, flow properties, and packing of the powder. To ensure uniformity and reproducibility, the powder samples were stored in moisture-controlled sealed containers at room temperature in the laboratory. The moisture content of each sample was measured before carrying out any tests or printing.

Physical and flow properties of powders. Standard tests were performed to determine the physical and flow properties of P. juliflora powders prepared from leaves, stems, and pods. Particle size fractions were obtained using a mechanical sieve (HAVER EML DIGITAL PLUS, Figure 9a in accordance with ASTM C136/C136M-19 [42], which provides standardized procedures for classifying fine and coarse aggregates. Based on the powder availability on the mesh sizes, three particle-size fractions of d < 355 µm for leaves and stems, and d < 500 µm for pods were chosen to assess the effect of particle size on flowability. Leaves and stems demonstrated moderate hygroscopicity, with moisture contents of ~ 8% and 9%, respectively, as measured by a KERN DAB moisture analyzer, and were stable under ambient conditions. Pod powders exhibited a lower moisture content of ~ 5% and were noted to be "sticky", indicating that the cohesion in powders may be attributable to surface chemistry rather than moisture content alone.

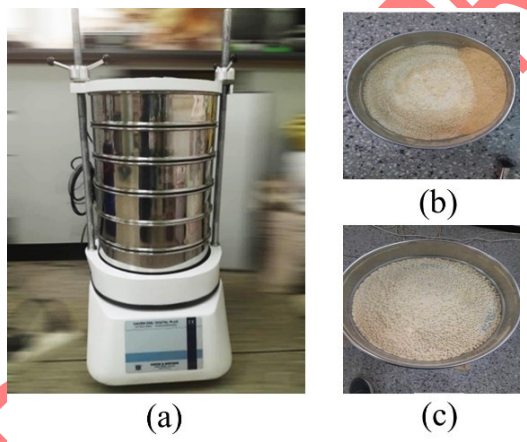

Figure 9. Mechanical sieving process: (a) Mechanical sieve shaker; (b) Fine and coarse pod powders after sieving; and (c) Adhered fine pod particles retained on larger mesh sizes.

Bulk density (DIN ISO 60) and tapped density (JEL STAV II) measurements indicated that leaves demonstrated consistent packing behaviour, while stems had slightly lower bulk and tapped density measurements. Pod powders showed higher bulk and tapped densities, although the sticky nature of the powders did not allow the bulk density measurement to be done easily without some effort to make the powder flow into the cylinder. This variation indicates how the flow characteristics of the biobased powders vary in each fraction of the powders. The results of the powder's physical characteristics are summarized in Table 3 and illustrated in Figure 10.

As can be seen from Figure 10a, flowability is dependent on the material fraction and the size of the particle. The flowability of leaf and stem powders was enhanced as the particle size increased. For the fine fractions, CI values around 22.5% for leaves and 27.4% for stems were obtained, whereas for the coarse fractions, values of 10.2% and 23.7% were determined, respectively. It implies that larger particles are more packed and have less cohesion.

Table 3. Physical and flow properties of Prosopis juliflora residue powders.

Material	Parameter

	Sieve size [µm]	Moisture content [%]	Bulk density [g/cm³]	Tapped density [g/cm³]	Carr Index [%]	Hausner Ratio
Leaves	< 90	8.09	0.380	0.490	22.483	1.290
	90-125	8.45	0.378	0.450	16.037	1.191
	125-355	8.28	0.377	0.420	10.198	1.114
Stems	< 90	9.07	0.203	0.280	27.357	1.377
	90-125	9.27	0.160	0.210	23.746	1.311
	125-355	9.02	0.175	0.230	23.710	1.311
Pods	90-125	5.17	0.470	0.580	19.000	1.235
	125-355	4.92	0.499	0.670	25.507	1.342
	355-500	5.05	0.513	0.650	21.041	1.266

On the other hand, pod powders, as shown in Figure 10b, exhibit erratic profiles, as both fine and coarse fractions present fair flowability with CI values of approximately 19% to 21%. The medium fraction, however, reaches a value of ~25.5%, indicative of poor flow, possibly due to agglomeration resulting from the shape of the particles. These results highlight the importance of particle morphology on flow performance, specifically for pod-based powders. Based on the standard powder classification for CI and HR in Section 2.2 (Table 1), the flowability revealed that leaf powders fall between "Excellent and Passable", stems between "Fair and Poor", and pods between "Fair and Poor". This variation indicates how the flow characteristics of the biobased powders vary in each fraction of the powders. These properties are important for binder jetting as they affect the powder-bed formation, interaction with the binder, and overall printability.

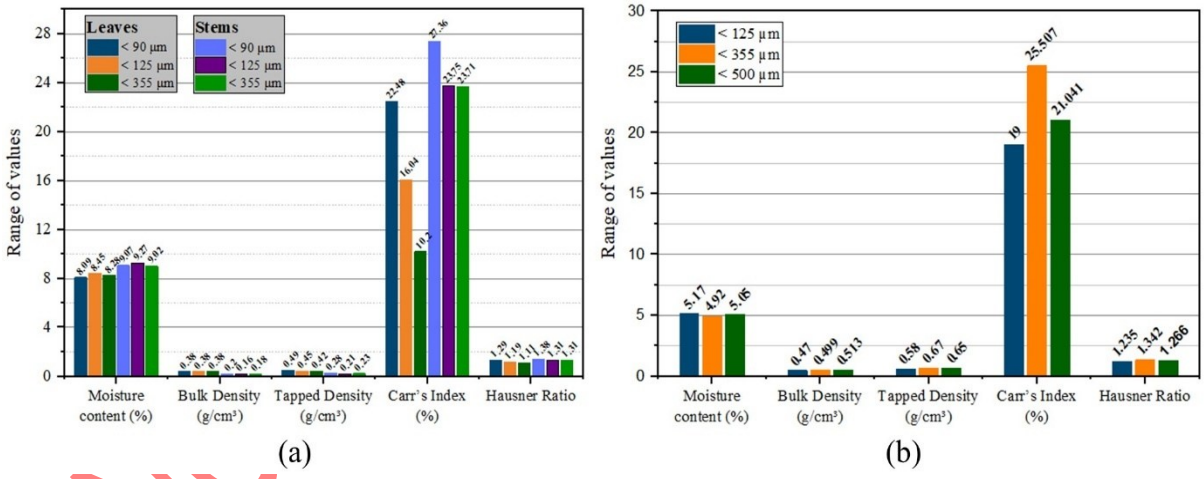

Figure 10. Physical and flow properties: (a) Leaf and stem powders; and (b) Pod powders.

Morphological analysis. The SEM images at different magnification levels show the powder characteristics of the P. juliflora residues. As observed in Figure 11a and 11b, angular and irregular particles with sharp edges and rough fractured surfaces. These particles can improve interlocking and packing, but they can also lead to increased friction during powder flow. Figure 11c and 11d illustrate elongated fibrous particles that are splintery in geometry, are coarsely striated, and have porous interiors; these are characteristic of plant fibers. The finer granular particles (Figure 11e and 11f) are smaller, more equiaxed, and less fibrous, but still irregular and porous. There is a presence of a greater tendency to agglomerate, which can negatively affect the flowability and packing uniformity of the powder [34]. In general, the presence of angular, fibrous, and granular shapes in the biobased powder is indicative of the heterogeneity of the material, which will affect spreading, packing density, and reaction with the binder during a binder jetting process.

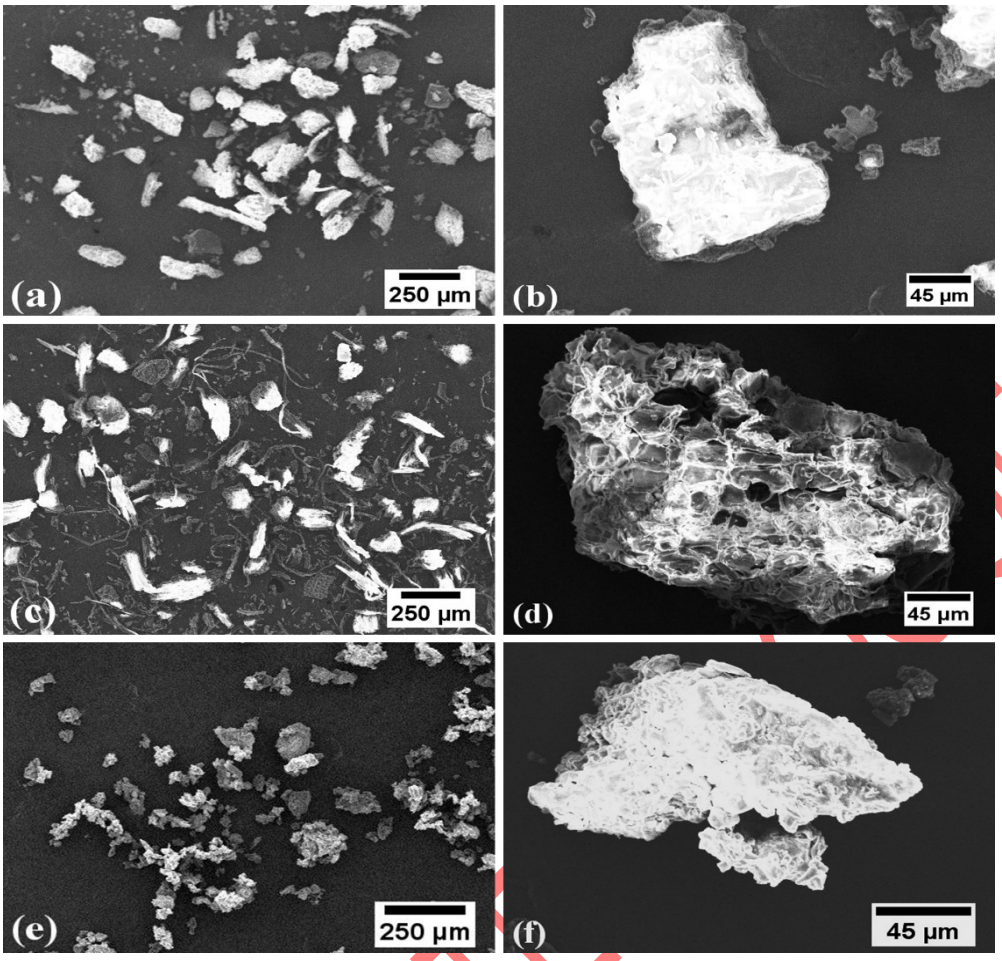

Figure 11. SEM images of Prosopis juliflora powder: (a-b) Leaves; (c-d) Stems; and (e-f) Pods.

Particle size distribution analysis. Particle size distribution (PSD) was conducted using laser diffraction to evaluate the size characteristics of the P. juliflora leaf, stem, and pod powders. The data summarized in Table 4 give the characteristic particle diameters D_{10}, D_{50}, and D_{90} of P. juliflora residues, powdered data using volume-based cumulative distribution (Q_3) and differential distribution (q_3). D_{10} denotes the particle size below which 10% of the total powder volume lies and is a measure of the fine fraction of the powder. D_{50} is the median-size of the particles and D_{90} is the particle size below which 90% of the particle volume is contained, representing the coarse fraction. The Q_3 and q_3 volume-based PSD curves are illustrated in Figure 12. The Q_3 curves show the cumulative contribution of particle sizes to the total powder volume, whereas the q_3 curves represent the frequency of particles at specific diameter ranges. Peaks in the q_3 curves indicate the most dominant particle size fractions.

The results show that all powders exhibited dominant particle sizes within the range of 20-110 µm. This particle size range is considered suitable for BJT applications as it provides a good balance between powder flowability and packing density. For example, at particle diameters close to the median values (D_{50}), the Q_3 curves reach approximately 50%, confirming the representative average particle size for each powder. Beyond this range, Q_3 increases gradually, while q_3 decreases, indicating a reduced population of coarse particles. This behaviour confirms that most particles are concentrated in the fine-to-medium size range, with fewer large particles contributing to the tail of the distribution. The median size of particles in pod powder was the highest, followed by 102.48 µm (D_{50}), whereas the leaf and stem powders were 60.23 µm and 52.24 µm, respectively.

Table 4. Particle size characteristics of Prosopis juliflora biobased residue powders.

Cumulative [%]	Diameter of leaves powder [µm]	Diameter of stems powder [µm]	Diameter of pods powder [µm]
D_{10}	7.74	10.25	10.19
D_{50}	60.23	52.24	102.48
D_{90}	232.62	177.84	286.74

The increased D_{50} and D_{90} values of the pod powder (D_{90} = 286.74 µm) also points to the fact that coarser particles are present, and the lengthy tail of the cumulative Q_3 curve to the right of the line indicates this fact also. It can be explained by the fact that the pods are fibrous and mechanically harder, which hinders the effective reduction in size when milling. In contrast, powders of leaves and stems showed finer distributions of particles. The stem powder had the smallest median diameter and less dispersion, as realized by the lower values of D_{50} and D_{90}. Conversely, the median size and distribution of leaf powder were a little larger than that of stem powder, indicating that the powder was not uniformly broken through grinding. The D_{90} of leaf powder (232.62 µm) was higher, which also proves that the coarse particles were present.

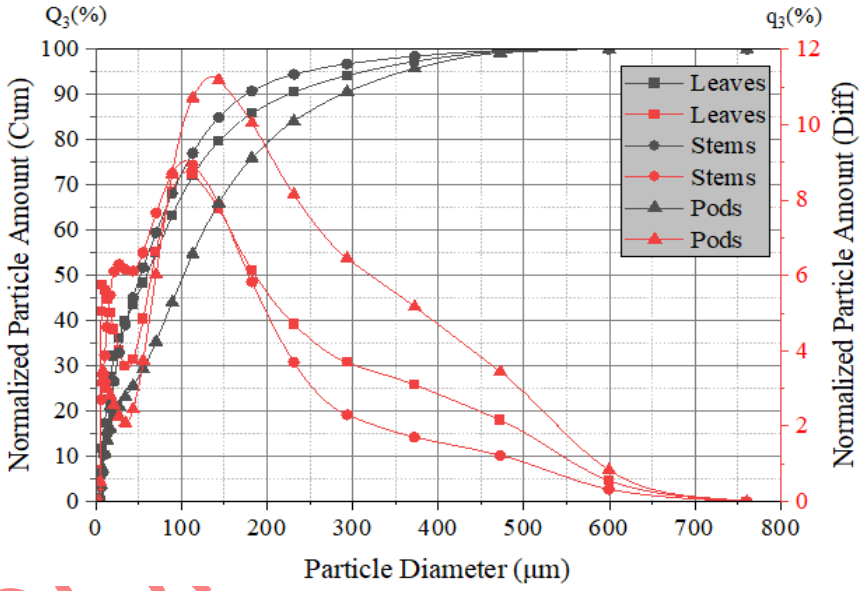

Figure 12. Volume-based Q_3 and q_3 PSD curves of Prosopis juliflora residue powders.

The difference PSD curves show a bimodal distribution of all powders with a definite number of fine and coarse particles. The bimodality is more enhanced in the leaf powder, which has a high fraction of ultrafine particles (d < 10 µm) and coarse particles (d > 200 µm). This could be caused by the heterogeneous microstructure of leaves, which consists of brittle tissues forming fines and tougher veins that cannot be broken easily.

Considering all results, the differences in the particle size properties that were observed indicate the impact that plant morphology has on the powder processing behaviour. These differences highlight the significance of controlling the size of particles and the type of material to be used in the production of P. juliflora powders that would be used to additively model products using 3D printing technology.

Powder-Bed Formation Assessment of Residue Materials in Binder Jetting

The leaf and stem-derived powders exhibited good spreading behavior in the "ZPrinter 310" 3D printer, enabling the formation of a smooth and continuous powder bed with uniform

layer thickness and consistency, as shown in Figure 13a and 13b. Consequently, these powders enabled us to successfully produce cube-shaped green parts with a stable geometry (Figure 14a and 14b). The powders originating from the pods, on the other hand, showed poor powder-bed formation and inconsistent layer deposition. Their stickiness resulted in problematic handling; during sieving, some particles would stick to the mesh of the sieve, and finer particles would build up within the coarser sieve fractions, as clarified in Section 3.1.1 (Figure 9b and 9c. The same problem occurred during the spreading process, as significant agglomeration also caused clumping and uneven spreading, thereby could not be formed continuous layers (Figure 13c).

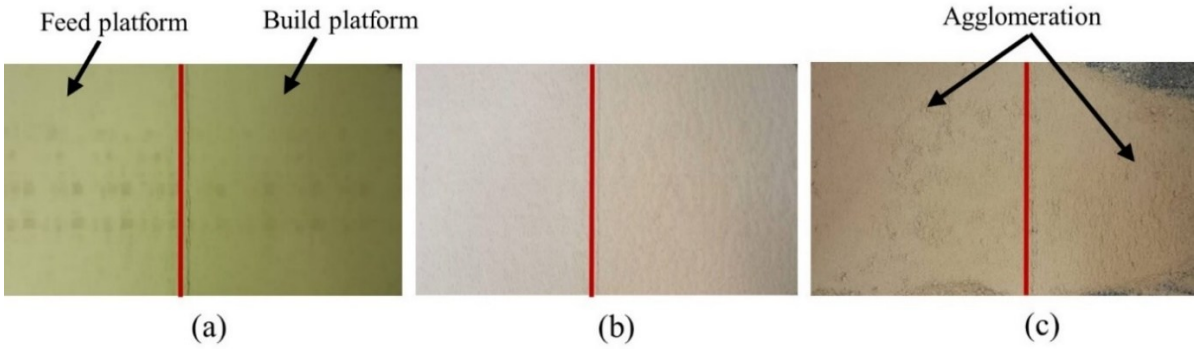

Figure 13. Powder spreadability evaluation images for: (a) Leaf; (b) Stem; and (c) Pod powders.

This behaviour not only hindered the formation of a uniform powder bed and caused uneven layer deposition but also resulted in caking beyond the intended CAD design boundaries, which makes it difficult to de-powder the intended shape from the unused powder, as illustrated in Figure 14c. The stickiness of the powders was a greater concern than particle size in limiting the use of pod-based powders. The specimens that were primarily produced from leaves and stems were evaluated for powder-bed formation, green-part integrity, and overall printing performance. No standardized mechanical testing was conducted, as it was not within the scope of the current study.

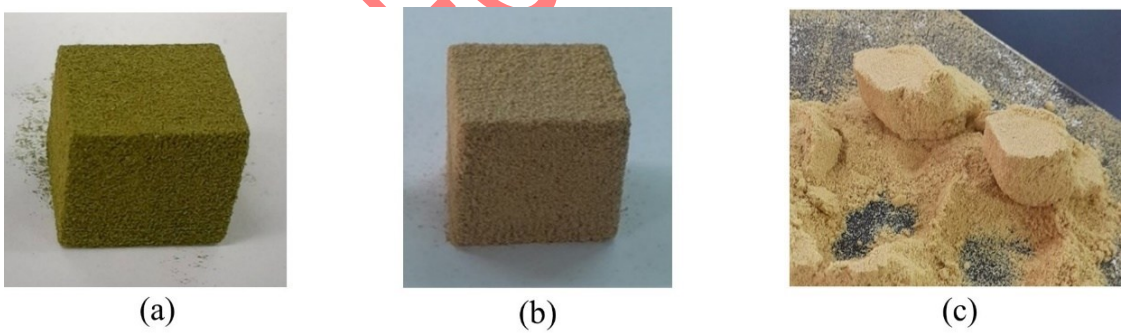

Figure 14. Printed green parts produced from: (a) Leaf; (b) Stem; and (c) Pod powders.

Justification of Prosopis Juliflora Residues for Binder Jetting Evaluation

The residue materials of P. juliflora were assessed for BJT owing to their physical, flow, morphological properties, PSD, and powder-bed formation behaviour. This section breaks down the observations according to the inherent material characteristics to give an overall explanation of the relative performance of the biobased residue materials. Leaf residues were found to be the most appropriate material. They had uniform sieving, good bulk and tapped densities, favourable flow indices, and angular to irregular particle shapes, which led to the successful layer formation and stable green parts. These characteristics could explain the formation of successful powder-bed, provide uniform layers, and maintain stable green parts observed in Section 3.2, highlighting the leaf residues being the most critical determinant of

BJT feasibility. The hard and fibrous nature of the stem residue powders, despite requiring labour-intensive preprocessing such as reducing to small chips, was identified as having slightly lower flowability, thereby being able to form continuous layers with acceptable printability. In contrast, pod residues were the least suitable. Although they exhibited higher bulk and tapped densities, the powders displayed strong agglomeration and stickiness, which hindered uniform spreading and powder-bed formation.

While the present study focused on processing powders in their natural state to establish baseline feasibility, the strong stickiness and agglomeration of pod-derived powders, due to surface sugars, oils, and extractives, remain a major limitation for processability. This behaviour indicates that the utilization of alternative pre-processing techniques like separating seeds from pods, using solvent extraction, or even mild alkali treatment might help overcome cohesion to improve powder flow, allowing for the incorporation of pod residues in BJT.

To quantify the overall suitability of the residue powders for BJT, a numerical scale was used between 1 and 5, with 1 representing inferior performance and 5 indicating excellent performance. Table 5 summarizes assigned ratings, indicating the material properties and their influence on the creation of powder beds and the integrity of powder beds.

Table 5. Suitability of Prosopis juliflora residue powders for binder jetting, based on powder characteristics and powder-bed formation (ratings: 1 = poor, 5 = excellent).

Property/Characteristics	Prosopis juliflora residue material		
	Leaves	Stems	Pods
Moisture content	4	4	5
Bulk and tapped density	4	3	4
Flow indices	4	3	3
Morphology	3	3	4
PSD	5	5	4
Powder-bed formation and layer consistency	5	5	2
Tendency to agglomerate	5	5	1
Overall suitability	5	4	2

Evaluation of Printability Using Paste Extrusion

The residues of P. juliflora exhibited a sticky nature on mixing with water, which adversely impacted their handling and printability. The prominent level of stickiness restricted the continuous extrusion of strands and the dimensional stability of the parts on the print bed. To overcome this problem, the P. juliflora powders were mixed with two different binder formulations. The higher the binder content in the powder blend, the lower the paste stickiness, as these bound particles together in a better way within the paste and provide greater internal bonding, forming more stable and extrudable pastes.

Another factor that was very essential in the behaviour of paste flow is the size of the particles. The fine size range of the particle was thus chosen with $d < 125$ µm, which allowed easier extrusion through the nozzle and minimized the chances of clogging. This size range also helped increase the homogeneity of the paste. The heating of the bed was not applied during printing to prevent early drying and to ensure a steady flow of paste during extrusion.

Moisture content and paste formulation characteristics. In all materials, there was a systematic rise in moisture content with a corresponding rise in binder content from 15 wt.% to 30 wt.%. The increased moisture content in 30 wt.% CMC can be explained by the hydrophilic character of CMC, which absorbs water and creates a viscous polymer network at high levels, thus raising the paste yield stress and the resistance to flow [43]. Table 6 sums up

the moisture content needed to gain homogeneous and extrudable pastes of each biobased fraction (Figure 15a-15c).

(a) (b) (c)

Figure 15. Paste preparation process from: (a) Leaf; (b) Stem; and (c) Pod powders.

The highest moisture content, with a maximum of 68% by total weight, was observed in stem-based pastes. These pastes showed resistance to extrusion at the lowest moisture levels. In contrast, the lowest moisture content was noted in pod-based pastes. A moisture content of 54 wt.% was the lowest at 15 wt.% CMC, with improved flowability of the paste material. These differences in moisture content, which depend on the P/B ratio formulation, directly affected extrusion stability and drying behavior.

Table 6. Prosopis juliflora paste formulations as used for paste extrusion 3D printing.

Material	Binder ratio (wt.%)	Moisture content (wt.%)
Leaf	15	56
	30	63
Stem	15	63
	30	68
Pod	15	54
	30	64

Effect of volumetric flow rate on extrusion stability and layer formation. The printability of the different biobased residues was investigated by varying the volumetric flow rate of the pastes from 40 mm^3/s to 64 mm^3/s. The impact of volumetric flow rate on the quality of the print is demonstrated using cylindrical and rectangular bar specimens. Figure 16 represents typical green-state prints of pod-based paste with 15 wt.% CMC. Both shapes of the specimens could be printed at the baseline flow rate of 40 mm^3/s (Figure 16a and 16b); nevertheless, the extrusion was not completely stable. The flow of the paste was not uniform, and local drying at the nozzle resulted in broken filaments, uneven layer deposition, and incomplete filling of the structured geometry. These characteristics show under-extrusion, which is due to insufficient material deposition in relation to the paste viscosity.

Extrusion stability and formation of layers improved dramatically when the flow rate was raised to 52 mm^3/s (Figure 16c and 16d). The filaments were deposited continuously, the layers were laid evenly, and the parts being printed were printed well. The rate at which the material flowed ensured a balance between material flow and nozzle motion, hence forming clear

cylindrical walls and better rectangular edges. This state provided an enhanced green-state structural integrity.

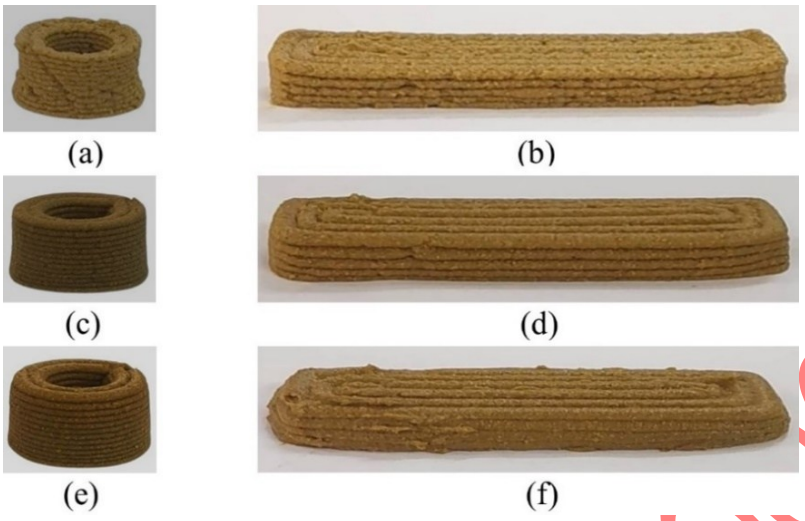

Figure 16. Green parts of pod-based paste at 15 wt.% CMC for cylindrical and rectangular bar specimens: (a-b) 40 mm^3/s; (c-d) 52 mm^3/s; and (e-f) 64 mm^3/s flow rates.

A further step of flow rate increase to 64 mm^3/s (Figure 16e and 16f) continued the extrusion process, but the deposition of high material caused over-extrusion. This resulted in compression of filaments, thickening of walls, and overfilling of print features. The rectangular bar specimens, especially, were of rounded sides and side lost sharp angles, whereas the cylindrical specimens were printable but had evidence of excess material deposition. formation. Though specimens were also satisfactorily printed at the entire range of flow rates, the best balance was found at a flow rate of 52 mm^3/s. This was despite the retention of surface continuity at the expense of general dimensional accuracy. In general, these findings indicate that in biobased MEX, a high volumetric flow rate affects the extrusion stability and the layer formation. Though specimens were also satisfactorily printed at the entire range of flow rates, the best balance of dimentional stability was found at a flow rate of 52 mm $^3/s$.

Drying behavior and dimensional stability of samples. During P. juliflora printing both the material fraction and P/B ratio had strong effects. Although minor environmental variability was noticed, the consistent room conditions allowed sufficient drying, maintaining dimensional stability and reproducible mechanical performance. Figure 17a-17d shows the typical dried samples of leaf and stem residues printed with 15 wt.% CMC and 52 mm^3/s flow rate. Stable drying behavior was observed in both leaf and stem-based specimens in both P/B ratio formulations. Despite moderate shrinkage of the 30 wt.% CMC, the printed samples still were in a structurally stable and dimensionally quantifiable condition. These residues had fibrous and particulate morphology, which probably decreased drying-induced stresses on the capillaries and thus, prevented undue deformation. No collapse was noticed, which means that the leaf and stem fractions are not as sensitive to the content of binder when drying.

On the contrary, the pod-based specimens were highly dependent on the binder ratio. Figure 18a demonstrates that specimens printed at 15 wt.% CMC maintained their geometric integrity and showed little shrinkage as they dried, such as cone formation in the case of cylindrical geometry, but remained functional. Nevertheless, samples printed at 30 wt.% CMC (Figure 18b) showed pronounced deformation during drying. In this case, the samples are characterized by inward wall collapse, rounding of edges, and partial closure of internal features, leading to dimensional instability and functional geometry loss. The greater the binder content, the more moisture was retained, and the capillary forces resulted in an inward wall deformation, causing internal features to collapse, and dimensional stability being lost.

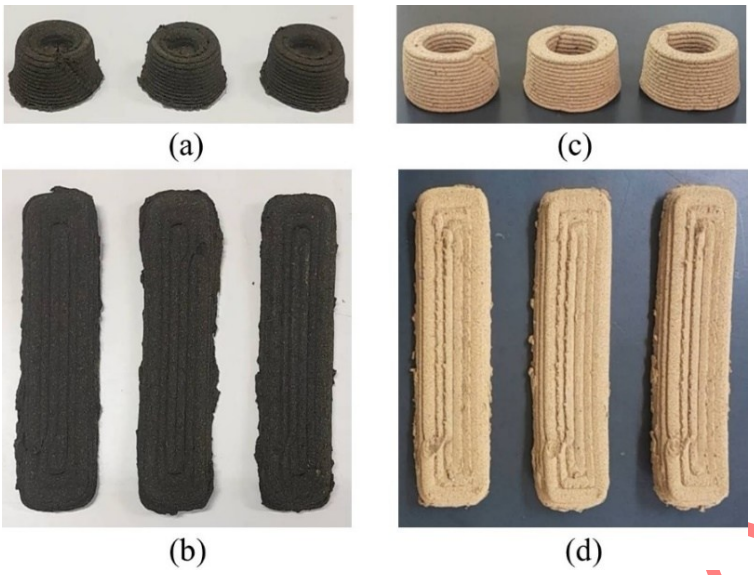

Figure 17. Dried printed samples at 15 wt.% CMC and 52 mm^3/s of flow rate for cylindrical and rectangular bars: (a-b) Leaf; and (c-d) Stem residues.

These findings reveal the important role of the binder content on drying stability and show that 15 wt.% CMC is better suited to pod-based materials. Overall, the minor environmental variations had little impact due to consistent laboratory conditions. The main factors that made a difference were the morphology of the material and the proportion of the binder, which shows how important the binder content is for stable drying.

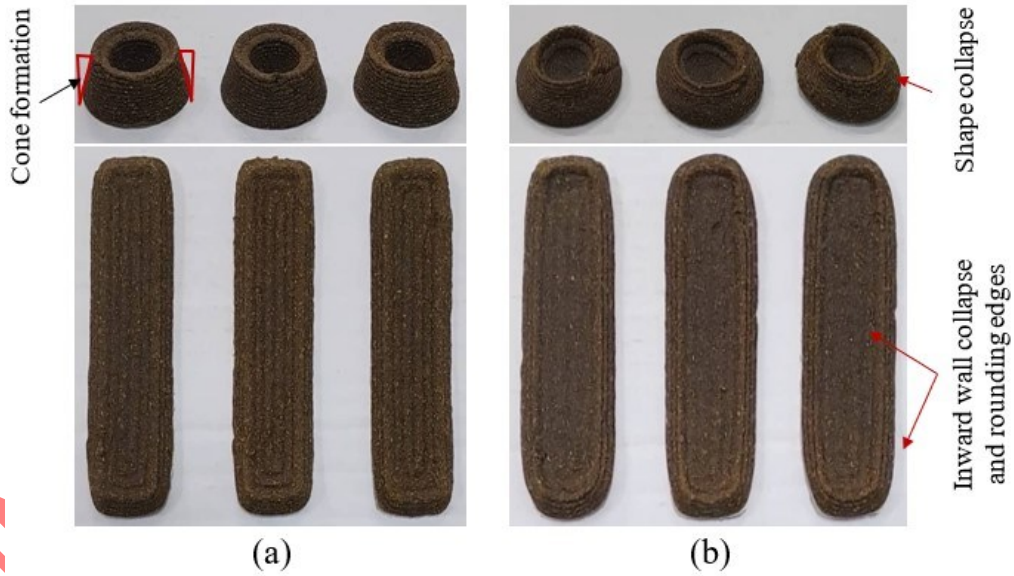

Figure 18. Dried pod specimens at 52 mm^3/s flow rate: (a) 15 wt.% CMC; and (b) 30 wt.% CMC.

Mechanical Testing of Paste-Extruded Samples

Compressive test. The compressive behaviour of the printed specimens was influenced by the material fractions (leaf, stem, and pod), P/B ratio, and flow rates. The findings of the two formulations are provided in Figure 19a and 19b. In leaf-based samples at 15 wt.% CMC, compressive strength decreased linearly with volumetric flow rate, with values of ~ 1.99 MPa at 40 mm^3/s flow rate and ~ 1.02 MPa at 64 mm^3/s flow rate. This observation indicated that there was poor layer definition and high internal defects as the flow rates increased, hence lowering load-bearing capacity. On the other hand, samples at 30 wt.% CMC showed a definite increase in compressive strength to 6.28 MPa at 52 mm^3/s flow rate and slightly decreased at

64 mm^3/s flow rate to 5.8 MPa. This tendency implies that high binder content promoted the particle bonding and interlayering cohesion until the optimal deposition level, after which over-deposition started to have an adverse effect on the structural integrity.

The compressive strength of the stem-based samples was the highest of all material fractions. At 15 wt.% CMC, the compressive strength was highest at 52 mm^3/s (nearly 6 MPa), slightly reduced at 64 mm^3/s, and lowest at mm^3/s (approximately 4.73 MPa). This shows enhanced densification and inter-layer bonding at a middle flow rate, at which point pore formation starts at over-deposition of the material. Nevertheless, at a higher level of binder contents of 30 wt.% CMC, a significant reduction in compressive strength was noted as the volumetric flow rate increased. As indicated in Figure 19b, compressive strength dropped with increased flow rate from ~ 10.17 MPa to 2.28 MPa. This loss is due to over-binding and moisture retention, leading to a weakening in the dried structure and making the internal voids easier to form.

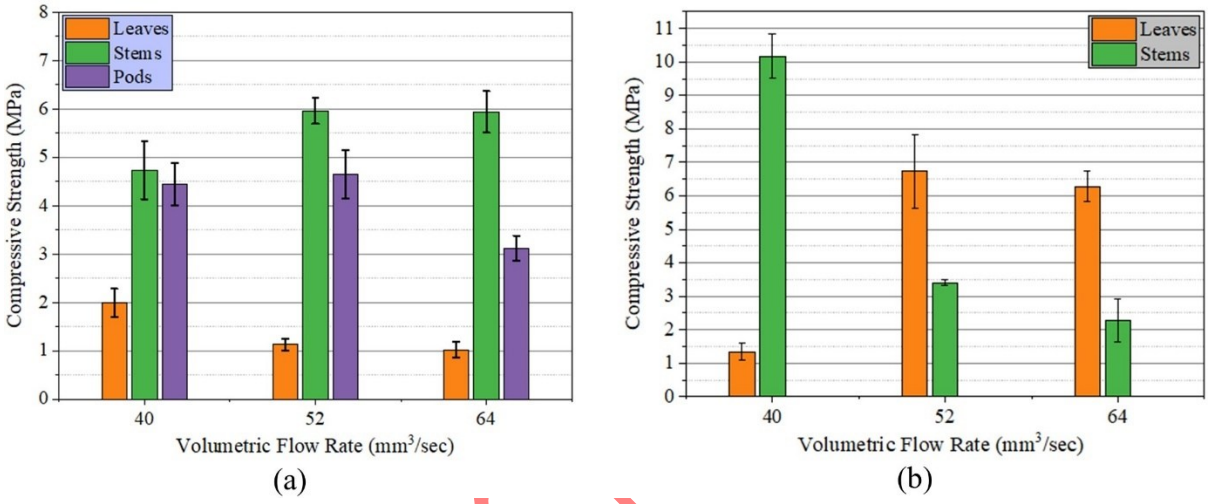

Figure 19. Compressive strength of printed samples: (a) 15 wt.% CMC; and (b) 30 wt.% CMC.

In the case of pod-based specimens, the compressive strength could be measured only at a ratio of 15 wt.% CMC as explained in Section 3.4.1.3. The compressive test was influenced by the volumetric flow rate, and it was maximum at the flow rate of 52 mm^3/s and slightly lower at the flow rate of 64 mm^3/s. This action signifies the increased consolidation and the rearrangement of particles, which was up to a certain level of flow rate, beyond which excessive deposition of the material caused a negative influence on the structural stability. At 30 wt.% CMC, samples were not able to sustain dimensional stability upon drying, and no quantifiable compressive strength was achieved.

Based on the results, compressive strength is highly regulated by both binder ratio and volumetric flow rate, and their influence are closely related to each other. Varying the binder ratio to 30 wt.% CMC increased the strength significantly, and in several cases resulted in higher compressive strength. However, this improvement did not occur for all materials and flow rates in the same way. Rather, the impact of binder content was based on the amount of material deposited as well as the plant fraction used. These findings indicate that the binder ratio cannot be assessed independently, as its influence on strength is also affected by volumetric flow rate and material.

Flexural test. Figure 20a and 20b showed that the flexural strength results of leaf, stem, and pod samples followed a similar pattern with the compressive tests, but highlighted different strengths. At 15 wt.% CMC, the best flexural strength was observed in pod-based samples with the highest flexural strength of ~ 5.69 MPa at 40 mm^3/s flow rate, whereas upon increasing to 52 mm^3/s and 64 mm^3/s, the flexural strength of the specimens declined to ~ 4.17 and 3.33 MPa, respectively. This decrease suggests that the increased flow rate can cause misalignment

of particles or internal voids that can decrease the capacity of the material to withstand bending. Stem-based samples exhibited moderate flexural strength (~ 2.86 MPa to 3.11 MPa) with a small rise at the 52 mm^3/s flow rate and a small drop at the 64 mm^3/s flow rate. This indicates enhanced layers deposition at moderate flow rates and development of structural defects at higher flow rates. In leaf-based samples, the least flexural strength (~ 1.34 MPa to 2.61 MPa) was recorded, showing a minimal contribution to mechanical resistance in bending.

There was a significant increase in overall flexural strengths at 30 wt.% CMC, and with stems, pods, and leaves recording the highest flexural strengths of 13.45 MPa, 9.44 MPa, and 4.94 MPa, respectively. Increased binder content enhanced the particle cohesion and matrix-particle interaction to stabilize the performance between volumetric flow rates and limited sensitivity to flow-induced defects. Remarkably, the relative contribution of powder type varied with binder content; pods gave better results at low CMC, with stems giving better flexural at high CMC, which explains the importance of the density of the matrix in the transfer of loads and ensuring structural integrity.

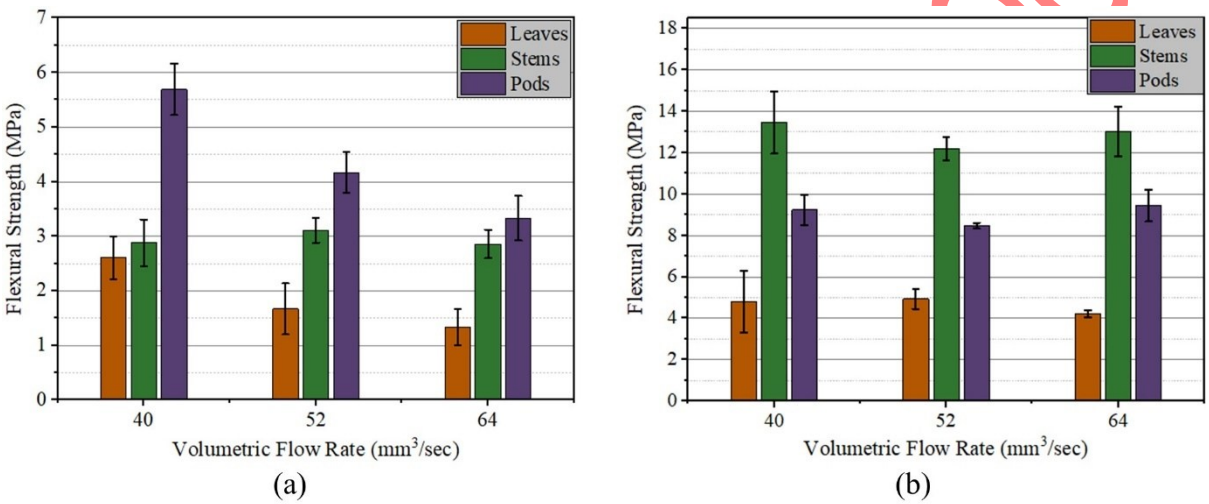

Figure 20. Flexural strength of printed samples: (a) 15 wt.% CMC; and (b) 30 wt.% CMC.

In summary, the flexural strength is influenced by both binder ratio and volumetric flow rate, and there are material fraction effects. The lower binder ratio is more dependent on flow rate, and the higher binder ratio is more likely to enhance flexural strength and diminish the effect of deposition rate. These results reveals that the bending behaviour is a result of the combined effects of material composition, binder percentage, and processing parameters, rather than on a single factor alone.

CONCLUSION(S)

In this study, the process feasibility and mechanical performance of P. juliflora biobased residue materials as alternative feedstocks for AM through BJT and MEX processes were investigated. From the analysis of experimental results, it can be concluded that:

- Material properties: It was observed that leaf and stem powders had better physical characteristics such as packing, flowability, and PSD. On the other hand, pod powders showed greater cohesion and tendency for agglomeration, resulting in poor powder-bed formation and inconsistent drying behaviour of paste-extruded parts.
- Powder-bed formation (BJT): Leaf and stem powders showed good spreadability and powder-bed formation, resulting in stable green parts. However, pod powders did not spread uniformly and could not be printed successfully under the tested conditions. These results suggest that process-level printability in BJT depends primarily on the powder morphology and flow properties.

- Paste-extrudability (MEX): In the MEX process, all fractions achieved stable extrusion and shape retention at the optimal volumetric flow rate of 52 mm^3/sec. Higher binder content improved dimensional stability and overall mechanical performance, although pod-based materials performed poorly in compressive tests.
- Mechanical performance: Paste-extruded components were found to have quantifiable mechanical tests. The peak compressive strength of 10.17 MPa was achieved in stem-based specimens, representing a 50.9% increment over the leaf-based parts and a 119.2% increment over the pod-based specimens. Likewise, the highest flexural strength was 13.45 MPa with the stem-based samples, which corresponds to 172.3% increment to the leaf-based parts and 42.5% increment to the pod-based samples. Increasing the binder content enhanced inter-particle bonding and mechanical properties across all fractions.
- Sustainability and economic relevance: This work shows how the invasive species P. juliflora can be valorized to usable AM materials by a simple and environmentally benign processing pathway, managing invasive species and promoting the principles of the circular economy.
- Featured application: The developed biobased materials can be used in low-load bearing components, packaging, and prototyping applications where moderate mechanical performance, low density, and low-cost of production are required.

In summary, this study is the first time to show that P. juliflora residue materials can be utilized as a viable, low-cost, and eco-friendly raw material for AM technologies. Leaf powder proves to be the most suitable filler material for BJT due to its excellent flowability and uniform layer formation, followed by stem powder, while stem-based materials showed outstanding performance in MEX owing to their fibrous structure. All fractions yielded printable components with satisfactory mechanical properties in MEX, whereas the mechanical properties of paste extrusion-printed parts largely depend on the material used, the amount of binder present, and the printing conditions. The findings provide a solid foundation for ongoing research work on detailed mechanical testing and optimization of binder-jetted parts, including post-processing, surface treatment techniques, and long-term durability and biodegradability of materials. These research directions will further support the potential of P. juliflora plant residues as a sustainable biobased material to be processed into AM and promote the development of environmentally responsible manufacturing solutions.

ACKNOWLEDGMENT(S)

The authors would like to acknowledge the financial support of the African Union (AU) through the Pan African University Institute for Basic Sciences, Technology and Innovation (PAUSTI); the Mechanical and Mechatronic Engineering Department at Jomo Kenyatta University of Agriculture and Technology (JKUAT), Kenya, for technical and laboratory assistance; and Raya University, Ethiopia, for sponsoring the study to attend abroad.

REFERENCES

[1] M. Srivastava, S. Rathee, V. Patel, A. Kumar, P.G. Koppad, A review of various materials for additive manufacturing: Recent trends and processing issues, J. Mater. Res. Technol. 21 (2022) 2612–2641. https://doi.org/10.1016/j.jmrt.2022.10.015.

[2] S. Saleh Alghamdi, S. John, N. Roy Choudhury, N.K. Dutta, Additive Manufacturing of Polymer Materials: Progress, Promise and Challenges, Polymers (Basel). 13 (2021) 753. https://doi.org/10.3390/polym13050753.

[3] M. Tebianian, S. Aghaie, N. Razavi Jafari, S. Elmi Hosseini, A. Pereira, F. Fernandes, M. Farbakhti, C. Chen, Y. Huo, A Review of the Metal Additive Manufacturing Processes, Materials (Basel). 16 (2023) 7514. https://doi.org/10.3390/ma16247514.

[4] M. Kamran, A Comprehensive Study on 3D Printing Technology, MIT Int. J. Mech. Eng. 6 (2016) 63–68.

[5] N.S. Reddy, H. Koti, P.M. Sajid, C.M. Velu, S.K. Velagaleti, P.L. Prasanna, K. Balasaranya, N. Rajeswaran, Sustainable AI-Driven Hybrid Manufacturing Using Additive and Subtractive Processes, Eng. Technol. Appl. Sci. Res. 15 (2025) 28878–28884. https://doi.org/10.48084/etasr.11785.

[6] A. Alghamdi, Enhancing 3D Printing Workflows through Multi-Objective Optimization and Reinforcement Learning Techniques, Eng. Technol. Appl. Sci. Res. 15 (2025) 21300–21305. https://doi.org/10.48084/etasr.10101.

[7] R. Sekula, A. Leis, A. Wassong, A. Preuss, H. Hanning, J. Kemnitzer, M. Wimmer, M. Kuniewski, P. Mikrut, Additive Manufacturing of Biobased Material Used in Electrical Insulation: Comparative Studies on Various Printing Technologies, Polymers (Basel). 17 (2025) 2248. https://doi.org/10.3390/polym17162248.

[8] J. Su, W.L. Ng, J. An, W.Y. Yeong, C.K. Chua, S.L. Sing, Achieving sustainability by additive manufacturing: a state-of-the-art review and perspectives, Virtual Phys. Prototyp. 19 (2024). https://doi.org/10.1080/17452759.2024.2438899.

[9] H. Jiang, X. Yang, H. Wang, Preparation and characterization of starch-based binders for binder jetting, RSC Adv. 14 (2024) 32506–32516. https://doi.org/10.1039/D4RA05411C.

[10] N.H. Mohd Yusoff, C.H. Chong, Y.K. Wan, K.H. Cheah, V.-L. Wong, Optimization strategies and emerging application of functionalized 3D-printed materials in water treatment: A review, J. Water Process Eng. 51 (2023) 103410. https://doi.org/10.1016/j.jwpe.2022.103410.

[11] Y. Ma, J. Potappel, M.A.I. Schutyser, R.M. Boom, L. Zhang, Quantitative analysis of 3D food printing layer extrusion accuracy: Contextualizing automated image analysis with human evaluations, Curr. Res. Food Sci. 6 (2023) 100511. https://doi.org/10.1016/j.crfs.2023.100511.

[12] L. Micke, L. Kühnel, W. Mwangi, K. Karanja, H. Zeidler, Conversion of bio-based residues into AM materials as a sustainable and cost-effective approach: example of water hyacinths in Kenya, in: Proc. 2023 Rapid.Tech Fachkongress Conf., Scientific article, Erfurt Messe, Germany, 2023: pp. 1–9.

[13] F. Khan, M. Shakil Arman, J. Sanders, M. Meraj Pasha, A. Mazedur Rahman, Z. Pei, T. Dong, Binder Jetting 3D Printing Utilizing Waste Algae Powder: A Feasibility Study, Intell. Sustain. Manuf. 1 (2024) 10016–10016. https://doi.org/10.70322/ism.2024.10016.

[14] M.H. Hussein, L.M. Mutava, D.W. Waititu, J.K. Kimotho, W. Mwangi, L. Micke, E.K. Ronoh, S.K. Karanja, Investigation of Mechanical Properties of Printed Rice Husk Parts Using an Inhouse Modified Paste Extrusion Printer, in: Proc. 2023 Sustain. Res. Innov. Conf., Kenya, 2023: pp. 1–5.

[15] M.N. Andanje, J.W. Mwangi, B.R. Mose, S. Carrara, Development of additive manufacturing biofilaments from recycled high-density polyethylene and rice husks: optimization of extrusion parameters, J. Agric. Sci. Technol. 23 (2024) 90–102. https://doi.org/10.4314/jagst.v23i4.6.

[16] M.B. Bah, J.W. Mwangi, K. Kabini, Fused Filament Fabrication of Recycled HDPE and Cactus Composite as a Biobased Material, Eng. Reports 7 (2025) e70121. https://doi.org/10.1002/eng2.70121.

[17] M.S. Santhosh, G. Karthikeyan, R. Sasikumar, R. Hariharan, R. Mohanraj, Mechanical and morphological behaviour of rice husk/prosopis juliflora reinforced bio composites, Mater. Today Proc. 27 (2020) 556–560. https://doi.org/10.1016/j.matpr.2019.12.021.

[18] D. SUBBIAH, N. MANI, S. SELVARAJU, E. THANGAVELU, Characterization and Analysis of Mechanical and Morphological Properties of Hybrid Composite Material from Prosopis Juliflora and Phoenix Sylvestris for Engineering Applications, Mater. Sci. (2024). https://doi.org/10.5755/j02.ms.37897.

[19] H.A. Debella, V.R. Ancha, S.M. Atnaw, Production, optimization, and characterization of Ethiopian variant Prosopis juliflora based biodiesel, Heliyon 9 (2023) e15721.

https://doi.org/10.1016/j.heliyon.2023.e15721.

[20] T.S.S.B. Rao, M. Gnanaprakasam, R. Manimaran, D. Balasubramanian, U. Kale, A. Kilikevičius, Sustainable synthesis and advanced optimization of Prosopis juliflora biomass catalyst for efficient biodiesel production and environmental impact assessment, Sci. Rep. 15 (2025) 4472. https://doi.org/10.1038/s41598-025-88355-z.

[21] X. Fang, Y. Zu, Q. Ma, J. Hu, State of the art of metal powder bonded binder jetting printing technology, Discov. Mater. 3 (2023). https://doi.org/10.1007/s43939-023-00050-w.

[22] M.I. Hussain, R. Shackleton, A. El-Keblawy, L. González, M.M. Trigo, Impact of the Invasive Prosopis juliflora on Terrestrial Ecosystems, in: Springer Nature Switzerland AG, 2021: pp. 223–278. https://doi.org/10.1007/978-3-030-73245-5_7.

[23] A. Al-Assaf, M.J. Tadros, S. Al-Shishany, S. Stewart, M. Majdalawi, M. Tabieh, Y.A. Othman, Economic Assessment and Community Management of Prosopis juliflora Invasion in Sweimeh Village, Jordan, Sustainability 12 (2020) 8327. https://doi.org/10.3390/su12208327.

[24] J. Mungoche, O.V. Wasonga, D. Ikiror, H. Akala, C. Gachuiri, G. Gitau, Prosopis juliflora (sw.) DC in the drylands: A review of invasion, impacts and management in Eastern Africa, Sustain. Environ. 11 (2025). https://doi.org/10.1080/27658511.2025.2521946.

[25] S.V. Pasha, C.S. Reddy, Global spatial distribution of Prosopis juliflora - one of the world's worst 100 invasive alien species under changing climate using multiple machine learning models, Environ. Monit. Assess. 196 (2024) 196. https://doi.org/10.1007/s10661-024-12347-1.

[26] V. Kishoin, W. Tumwesigye, B. Turyasingura, W. Wilber, P. Chavula, J.P. Gweyi-onyango, S. Kader, V. Spalevic, G. Skataric, L. Jaufer, The negative and positive impacts of Prosopis juliflora on the Kenyan and Ethiopian ecosystems: A review study Violah, Not. Sci. Biol. 16 (2024) 1–15. https://doi.org/10.15835/nsb16111832.

[27] B.-J. Gu, J. Wang, M.P. Wolcott, G.M. Ganjyal, Increased sugar yield from pre-milled Douglas-fir forest residuals with lower energy consumption by using planetary ball milling, Bioresour. Technol. 251 (2018) 93–98. https://doi.org/10.1016/j.biortech.2017.11.103.

[28] K.& S. GmbH, Operating Manual – Moisture Analyzer DAB 100-3, Version 1.3, (2018). https://manualzz.com/doc/81329855/kern-dab-moisture-analyser-operating-manual, [Accessed: 08-July-2025].

[29] A. International, Test Methods for Apparent Density, Bulk Factor, and Pourability of Plastic Materials, (2017) 6. https://doi.org/10.1520/D1895-17.

[30] S.E.I. 60:2023, Plastics - Determination of apparent density of material that can be poured from a specified funnel (ISO 60:2023), Geneva, 2023. https://standards.iteh.ai/catalog/standards/cen/cd643f0f-d001-4f71-8be8-6e51f78a394e/en-iso-60-2023, [Accessed: 09-July-2025].

[31] ISO 3953:2025(en), Metallic powders — Determination of tap density, 2025. https://www.iso.org/obp/ui/en/#iso:std:iso:3953:ed-5:v1:en, [Accessed: 09-July-2025].

[32] U.S.P. Convention, USP <1174> Powder Flow, 2024. https://www.usp.org/harmonization-standards/pdg/general-chapters/powder-flow, [Accessed: 20-July-2025].

[33] PharmaSciences, Compressibility Index and Hausner Ratio, (2022). https://pharmasciences.in/compressibility-index-and-hausner-ratio/, [Accessed: 20-July-2025].

[34] S.F. Islam, S.M. Hawkins, J.L.L. Meyer, A.R.C. Sharman, Evaluation of different particle size distribution and morphology characterization techniques, Addit. Manuf. Lett. 3 (2022) 100077. https://doi.org/10.1016/j.addlet.2022.100077.

[35] A.P. Clares, G. Manogharan, Discrete-Element Simulation of Powder Spreading Process

in Binder Jetting, and the Effects of Powder Size, in: Vol. 1 Addit. Manuf. Adv. Mater. Manuf. Biomanufacturing; Life Cycle Eng. Manuf. Equip. Autom., American Society of Mechanical Engineers, 2021: p. V001T01A009. https://doi.org/10.1115/MSEC2021-63351.

[36] X. Lv, F. Ye, L. Cheng, S. Fan, Y. Liu, Binder jetting of ceramics: Powders, binders, printing parameters, equipment, and post-treatment, Ceram. Int. 45 (2019) 12609–12624. https://doi.org/10.1016/j.ceramint.2019.04.012.

[37] J. Huang, L. Li, 3D printing of cellulose-based biomaterials: A review, BME Horiz. 3 (2025) 138--138. https://doi.org/10.70401/bmeh.2025.0001.

[38] I. Albelo, R. Raineri, S. Salmon, Materials and Methods for All-Cellulose 3D Printing in Sustainable Additive Manufacturing, Sustain. Chem. 5 (2024) 98–115. https://doi.org/10.3390/suschem5020008.

[39] L. Lendvai, I. Fekete, D. Rigotti, A. Pegoretti, Experimental study on the effect of filament-extrusion rate on the structural, mechanical and thermal properties of material extrusion 3D-printed polylactic acid (PLA) products, Prog. Addit. Manuf. 10 (2025) 619–629. https://doi.org/10.1007/s40964-024-00646-5.

[40] F. Hu, T. Mikolajczyk, D.Y. Pimenov, M.K. Gupta, Extrusion-Based 3D Printing of Ceramic Pastes: Mathematical Modeling and In Situ Shaping Retention Approach, Materials (Basel). 14 (2021) 1137. https://doi.org/10.3390/ma14051137.

[41] A. International, Standard Test Methods for Flexural Properties of Unreinforced and Reinforced Plastics and Electrical Insulating Materials, Los Angeles, CA, USA, 2017. https://www.universalgripco.com/astm-d790, [Accessed: 05-October-2025].

[42] I.O. for Standardization, Coating powders: Determination of particle size distribution by sieving, 2019. https://www.iso.org/standard/68393.html, [Accessed: 10-August-2025].

[43] I. Insua, O. Etzold, I. Calafel, R. Aguirresarobe, M. Calderón, M. Fernández, Rheological Insight into the 3D Printability of Carboxymethyl Cellulose-Based Hydrogels, Gels 11 (2025) 259. https://doi.org/10.3390/gels11040259.